

Determination of Single-Nucleon Wave Functions by Transverse Electron Scattering

R. S. Hicks, J. Button-Shafer, B. Debebe, J. Dubach, A. Hotta,^(a) R. L. Huffman,^(b) R. A. Lindgren,^(c)
and G. A. Peterson

Department of Physics and Astronomy, University of Massachusetts, Amherst, Massachusetts, 01003

R. P. Singhal

Kelvin Laboratory, Department of Physics and Astronomy, University of Glasgow, Glasgow, Scotland

and

C. W. de Jager

*Sektie Kernfysica, Nationaal Instituut voor Kernfysica en Hoge-Energiefysica,
1009 AJ Amsterdam, The Netherlands*

(Received 20 July 1987)

Transverse form factors have been measured for elastic electron scattering from ^{10}B and ^{11}B , as well as for the electroexcitation of the 1.74-MeV ($J^\pi=0^+$, $T=1$) and 5.17-MeV (2^+ , 1) levels of ^{10}B . These results were utilized to determine the radial shape of the $1p_{3/2}$ single-particle wave function within the nuclear interior.

PACS numbers: 25.30.Bf, 21.10.Ft, 25.30.Dh, 27.20.+n

Electron scattering is unequalled for the precise determination of nuclear charge distributions. Several attempts have been made to extend this technique to obtain information on the density distributions of individual nucleons within the nucleus. The first such study was made by Sinha *et al.*¹ who compared elastic Coulomb scattering from the isotones ^{39}K and ^{40}Ca . It was found that the ground-state charge-density difference could not be attributed solely to the extra $d_{3/2}$ proton in ^{40}Ca : The added proton also distorts the ^{39}K core by polarization. Clear differences observed between the charge distributions of *isotopes* confirm the importance of core polarization.² This effect obscures the interpretation of charge-density differences entirely in terms of single-nucleon wave functions.

This Letter reports a new determination of single-nucleon wave functions by a different approach, one based on *magnetic* electron scattering. Cross sections for magnetic scattering are strongly determined by nucleons in the outermost valence shells, and hence provide direct quantitative data on these orbits. As will be shown, by our confining attention to high-multipolarity "stretched" transition-matrix elements, involving only the highest-spin orbit within the valence shell, the radial shape of that orbit may be determined.³ Only the spin-flip one-body operator contributes, and so the analysis is relatively simple.⁴ Furthermore, core-polarization contributions to the measured cross sections are relatively small.

Previous analyses of high-multipolarity elastic magnetic cross sections for odd- A nuclei have provided precise information on the rms size of valence orbitals.⁵ However, in these cases the stretched-multipole contributions are partially obscured by contributions from lower multipoles, and it is not possible to deduce the

shape of the single-particle wave functions within the nuclear interior. This difficulty does not apply in the nearly unique case of the pure $M3$ electroexcitation of the ($J^\pi=3^+$, $T=0$) ground state of ^{10}B to the (0^+ , $T=1$) level at 1.74 MeV. In a $1p$ shell model with one-body operators, the form factor for this transition has the form

$$F_{M3}(q) \sim q \int_0^\infty |R_{p_{3/2}}(r)|^2 j_2(qr) r^2 dr, \quad (1)$$

where $R_{p_{3/2}}(r)$ is the $1p_{3/2}$ single-nucleon wave function. Since $|F_{M3}(q)|^2$ may be directly measured over a large range of the momentum transfer q , Eq. (1) may be transformed to reveal details of the distribution of the $1p_{3/2}$ single-nucleon orbit.

Accordingly, measurements of this form factor were made with use of the electron-scattering facility of the Bates-MIT Linear Accelerator Center. Electrons scattered at 150° and 180° from ^{10}B and ^{11}B targets were counted for incident beam energies between 203 and 416 MeV, corresponding to $q=2.0$ to 3.9 fm^{-1} . The targets consisted of isotopically enriched powders supported by thin graphite foils. The targets were relatively thick, approximately 300 mg cm^{-2} , to ensure the measurability of the small cross sections encountered at high q . Useful data⁶ were acquired for magnetic elastic scattering from both nuclei and for the 1.74- and 5.17-MeV transitions in ^{10}B .

The new data are displayed in Fig. 1, as are previous results⁷⁻¹⁰ at lower q . Longitudinal $C0$ and $C2$ contributions to the present ^{10}B and ^{11}B elastic measurements were subtracted by our utilizing the results of Stovall *et al.*¹¹ In the case of ^{10}B such contributions were less than 20%. For ^{11}B , which has much larger magnetic elastic cross sections, the $C0$ and $C2$ components were less than

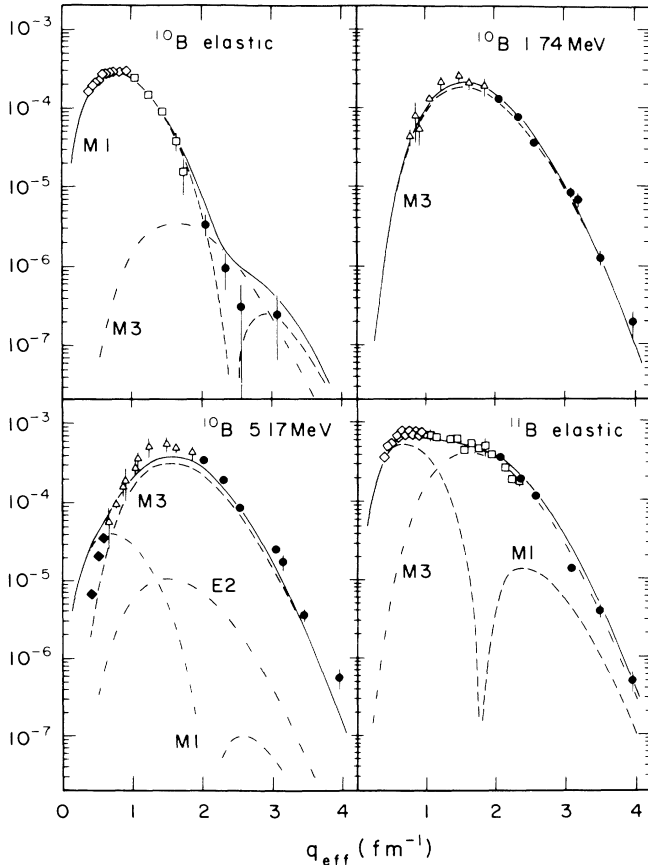


FIG. 1. Transverse electron-scattering form factors for ^{10}B and ^{11}B plotted as functions of the effective momentum transfer q_{eff} (Ref. 11). The data shown are from this experiment (circles), Rand *et al.*, Ref. 7 (squares), Fagg *et al.*, Ref. 8 (filled lozenges) Lapikas, Ref. 9 (open lozenges), and Ansaldo *et al.*, Ref. 10 (triangles). The curves represent theoretical predictions, obtained with use of the $1p$ -shell amplitudes of Cohen and Kurath (Ref. 12) and single-particle wave functions derived from a Woods-Saxon potential well. The total calculated form factors, represented by the continuous curves, also include one-pion-exchange-current contributions (Ref. 13).

1%.

In Fig. 1 the data are compared to the results of shell-model calculations that employ the $1p$ -shell amplitudes of Cohen and Kurath¹² and single-nucleon wave functions derived from a Woods-Saxon potential well of radius $r_{\text{WS}}=2.14$ fm and standard diffuseness $a=0.70$ fm in the relative core-particle coordinate system.¹⁴ The total calculated form factors also include one-pion-exchange currents¹³ obtained with use of harmonic-oscillator wave functions with size $b_{\text{rel}}=1.63$ fm. The choice of reasonable nuclear well parameters was the only freedom exercised. There was no renormalization in any way: Bare-nucleon charges and magnetic moments were employed. Generally sound quantitative agreement exists between experiment and theory, even

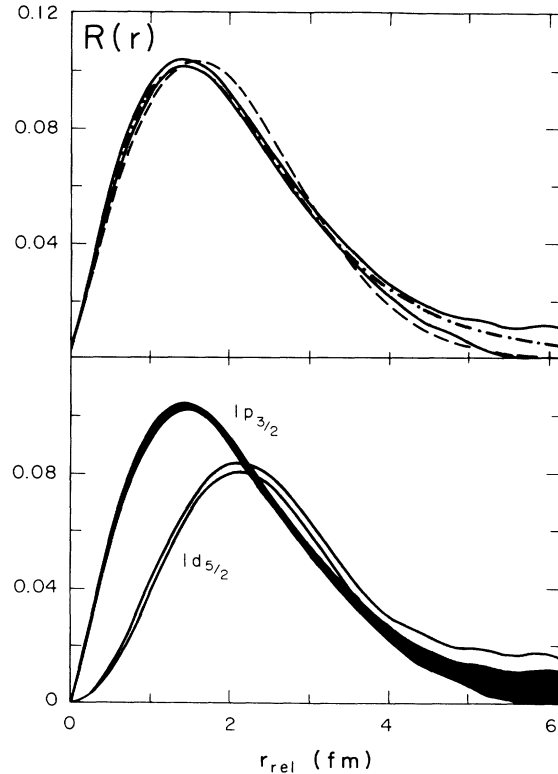


FIG. 2. Top: The shaded band represents the $1p_{3/2}$ single-particle wave function extracted from the measured 1.74-MeV $M3$ form factor in ^{10}B . The width of the band indicates the error due to the statistical uncertainties and incompleteness of the measured data (Ref. 16). The dashed curve shows the harmonic-oscillator shape ($b_{\text{rel}}=1.60$ fm); the dot-dashed curve is obtained from a Woods-Saxon potential well ($r_{\text{WS}}=1.59$ fm, $a=0.90$ fm, $V_0=-91$ MeV, and $V_{\text{s.o.}}=0.0$ MeV). Bottom: Comparison of the deduced $1p_{3/2}$ wave function with the wave function determined for the $1d_{5/2}$ neutron orbit in ^{13}C . The abscissa for both graphs is the relative core-particle separation and the normalization of the wave functions is such that $4\pi\int_0^\infty |R(r)|^2 r^2 dr = 1$.

for the highest momentum transfers.

As a first step in our obtaining the $1p_{3/2}$ single-particle wave function from the 1.74-MeV $M3$ form factor, the data were corrected for distortion of the incoming and outgoing waves by means of an iterative procedure.¹⁵ Small calculated exchange-current contributions were then removed from the data. Finally, the single-nucleon wave function $R_{p_{3/2}}(r)$ was extracted in the relative core-particle coordinate system¹⁴ with use of the Fourier-Bessel (FB) expansion technique¹⁶ with a cutoff radius of 6.5 fm. Smearing of the wave function arising from the finite size of the nucleon was removed by means of a four-pole expansion.¹⁷

Figure 2 shows that the resultant $1p_{3/2}$ wave function is well determined for $r_{\text{rel}} < 4$ fm. The error in the wave

function grows at larger distances, in large part because of the lack of precise data below $q = 2 \text{ fm}^{-1}$. In order to damp the oscillations incipient at this point in an unconstrained FB analysis, the shape of the fitted wave function has been biased¹⁶ with a Woods-Saxon dependence beyond $r_{\text{rel}} = 4 \text{ fm}$. The imposition of this bias raises the χ^2 value per degree of freedom from 0.62 to 0.95, with most of the increase coming from the four form-factor points measured above $q = 3 \text{ fm}^{-1}$. The spacing of these points is comparable to the separation of the peak contributions of individual terms in the FB expansion,¹⁶ and the unconstrained fit follows the statistical fluctuations in the data. With such a large- r "tail" bias, a smoother curve is forced through these data, more in accord with expectations. Note that the tail bias has little effect on the shape deduced for the wave function at $r < 4 \text{ fm}$, which constitutes the main focus of this paper.

The deduced wave function represents an average of the proton and neutron orbits, but is weighted somewhat more heavily by the proton, since the contributions of the nucleons to the form factor are in proportion to their magnetic moments. Woods-Saxon calculations, identical except for different binding energies and Coulomb potentials, give proton and neutron wave functions of very similar shapes, both being easily accommodated within the error band shown in Fig. 2.

Analyses of the data were also made with use of Woods-Saxon shapes, as well as with generalized polynomial expansions based on the oscillator model.¹⁸ With χ^2 per degree of freedom < 0.68 , these representations also provide excellent fits to the data, and confirm the essential model independence of the deduced wave function at $r < 4 \text{ fm}$. Since such models are more restrictive than the FB analysis, the $R(r)$ deduced at larger radii are better defined, and an rms radius of $2.57 \pm 0.04 \text{ fm}$ was determined for the $1p_{3/2}$ orbital.

As indicated in Fig. 2, the extracted wave function is well fitted by the Woods-Saxon form, with a large diffuseness $a = 0.9 \pm 0.2 \text{ fm}$ being preferred. In contrast, the simple $1p_{3/2}$ oscillator wave function decreases too steeply beyond $r = 2 \text{ fm}$.

Support for the credibility of the deduced wave functions comes from the remarkably good theoretical description of all the data shown in Fig. 1 by the $1p$ -shell amplitudes of Cohen and Kurath. This suggests that higher excited orbitals are present only as small admixtures in the wave functions of the levels studied here. If such admixtures were large, the rationale underlying the extraction of the $1p_{3/2}$ wave function would be invalidated. In order to investigate this possibility further, additional shell-model calculations were performed in a complete $2\hbar\omega$ basis space. On balance, these more detailed calculations improve upon the already good agreement with the data. For example, the $M3$ component predicted for the ^{10}B elastic magnetic form factor is reduced by a factor of 2, and the $M1$ form factor in the 5.17-MeV

transition by a factor of 7, remedying two of the more obvious problems with the $1p$ -shell predictions. In the case of the 1.74-MeV excitation, the $2\hbar\omega$ calculations give a 9% decrease in the magnitude of the $M3$ form factor, slightly diminishing the quality of the fit. This decrease ensues largely from a simple reduction in the $1p_{3/2} \rightarrow 1p_{3/2}$ transition amplitude; the shape of the predicted $M3$ form factor is affected very little by the opening of the $2s-1d$ and $2p-1f$ shells. On the basis of these calculations, the neglect of the $2\hbar\omega$ configurations increases the $1p_{3/2}$ radial parameters r_{WS} and a , as well as the deduced rms size, but only by $\leq 2\%$. The effect lies comfortably within the uncertainties reflected by the error band in Fig. 2.

Further support for the validity of the deduced wave functions comes from the striking consistency seen in the shapes of the measured $M3$ form factors. In addition to the 1.74-MeV transition, the $M3$ component is also dominant in the excitation of the 5.17-MeV level, as well as in the ^{11}B elastic magnetic form factor above $q = 1.5 \text{ fm}^{-1}$. Least-squares fits to these data with use of Woods-Saxon wave functions gave respective rms sizes for the $1p_{3/2}$ orbit in the ratio 1.000:0.993:0.982. Since there exist $\approx 2\%$ errors in each case, the differences are not significant. Such consistency suggests that, for these low-lying states, the shape of the $1p_{3/2}$ wave function is relatively constant: Any changes arising from differences in single-particle binding energies must be small. Finally, it is noted that the calculated one-pion-exchange-current contribution has almost the same q dependence as the one-body part, and therefore has little influence on the extracted radial shape.

Given the determination of the $1p_{3/2}$ wave function, the distribution of the $1d_{5/2}$ orbit could be extracted from measurements of an $M4$ form factor for another stretched configuration:

$$F_{M4}(q) \sim q \int_0^\infty |R_{p_{3/2}}(r)R_{d_{5/2}}(r)| j_3(qr) r^2 dr.$$

Unfortunately, no $M4$ form factors have been measured in (e, e') experiments on ^{10}B . However, comprehensive data¹⁹ exist for the 9.50-MeV $M4$ neutron transition in ^{13}C . According to a shell-model interpretation¹⁴ of the ground-state charge distributions, the distance scale of the deduced ^{10}B wave function need only be increased by 1.8% to obtain the $1p_{3/2}$ neutron orbit in ^{13}C . The procedure previously described was then repeated to determine the ^{13}C $1d_{5/2}$ neutron wave function. Although the uncertainties due to the admixtures of higher excited orbitals and meson-exchange currents compound in this case, Fig. 2 shows this wave function to have the expected dependence, peaking at a larger distance than the $1p_{3/2}$ wave function. Nevertheless, it is clear that the $1d_{5/2}$ wave function extracted in this manner is more qualitative than the deduced $1p_{3/2}$ wave function.

In conclusion, the $1p_{3/2}$ single-particle wave function

has been determined from the stretched-multipole $M3$ form factor for the 1.74-MeV transition in ^{10}B . Regrettably, few opportunities for similar studies in other nuclei are known. For odd- A nuclei, there are numerous examples of stretched $0\hbar\omega$ multipoles, particularly for elastic scattering, but the associated form-factor components are invariably obscured by overlapping contributions from lower multipoles. Presently under development are facilities for the measurement of $(e, e'\gamma)$ and electron scattering from polarized nuclei, techniques which permit the separation of the various multipole components. Moreover, studies are being undertaken to understand better the final-state interactions which affect the interpretation of the $(e, e'p)$ reaction, where the cross section is proportional to the square of the wave function of the ejected proton. When these objectives are realized, electron-scattering studies will become a rich source of information on single-particle wave functions using the type of analyses outlined here.

We thank Dr. D. J. Millener for his advice. This work was supported by the U.S. Department of Energy, and in part belongs to the research program of the Nationaal Instituut voor Kernfysica en Hoge Energie Fysica (NIKHEF, Sectie K), which is funded by the Stichting voor Fundamenteel Onderzoek der Materie (FOM) and the Nederlandse Organisatie voor Zuiver Wetenschappelijk Onderzoek (ZWO).

^(a)Present address: Department of Liberal Arts, School of Physics, Shizuoka University, Shizuoka, Japan.

^(b)Present address: Department of Physics, Wittenberg University, Springfield, OH 45501.

^(c)Present address: Department of Physics and Astronomy, University of Virginia, Charlottesville, VA 22901.

¹B. B. P. Sinha *et al.*, Phys. Lett. **35B**, 217 (1971).

²H. Rothhaas, contribution to the Conference on Modern

Trends in Elastic Electron Scattering, NIKHEF-K, Amsterdam, 1978, edited by C. de Vries (unpublished).

³J. Heisenberg *et al.*, Phys. Rev. C **29**, 97 (1984), used a related approach utilizing measurements of *longitudinal* scattering from ^{90}Zr to extract the rms size of the $1g_{7/2}$ proton orbit. However, such an analysis could not completely isolate a single orbital, the data spanned a limited range of momentum transfer, and a relatively unconstrained determination of the single-particle wave function within the nuclear interior was not presented.

⁴R. A. Lindgren and F. Petrovich, in *Spin Excitations in Nuclei*, edited by F. Petrovich *et al.* (Plenum, New York, 1984).

⁵P. K. A. de Witt Huberts *et al.*, Phys. Lett. **71B**, 317 (1977).

⁶See American Institute of Physics Document No. PAPS PRVLT-60-905-4 for four pages of tabulated cross-section measurements and deduced wave functions. Order by PAPS number and journal reference from American Institute of Physics, Physics Auxiliary Publication Service, 335 East 45th Street, New York, NY 10017. The price is \$1.50 for each microfiche or \$5.00 for photocopies. Airmail additional. Make checks payable to American Institute of Physics.

⁷R. E. Rand *et al.*, Phys. Rev. **144**, 859 (1966).

⁸L. W. Fagg *et al.*, Phys. Rev. C **14**, 1727 (1976).

⁹L. Lapikas, in Ref. 2.

¹⁰E. J. Ansaldò *et al.*, Nucl. Phys. **A322**, 237 (1979).

¹¹T. Stovall *et al.*, Nucl. Phys. **86**, 225 (1966).

¹²S. Cohen and D. Kurath, Nucl. Phys. **73**, 1 (1965); the $1p$ -shell amplitudes were obtained using the (8-16)2BME interaction.

¹³J. Dubach, Nucl. Phys. **A340**, 271 (1980).

¹⁴D. J. Millener *et al.*, Phys. Rev. C **28**, 497 (1983), and private communication.

¹⁵U. Deutschmann *et al.*, Nucl. Phys. **A411**, 337 (1983).

¹⁶J. Heisenberg, in *Advances in Nuclear Physics*, edited by J. W. Negele and E. Vogt (Plenum, New York, 1981), Vol. 12, p. 61.

¹⁷G. G. Simon *et al.*, Nucl. Phys. **A333**, 381 (1980).

¹⁸R. S. Hicks *et al.*, Phys. Rev. C **36**, 485 (1987).

¹⁹R. S. Hicks *et al.*, Phys. Rev. C **34**, 1161 (1986).

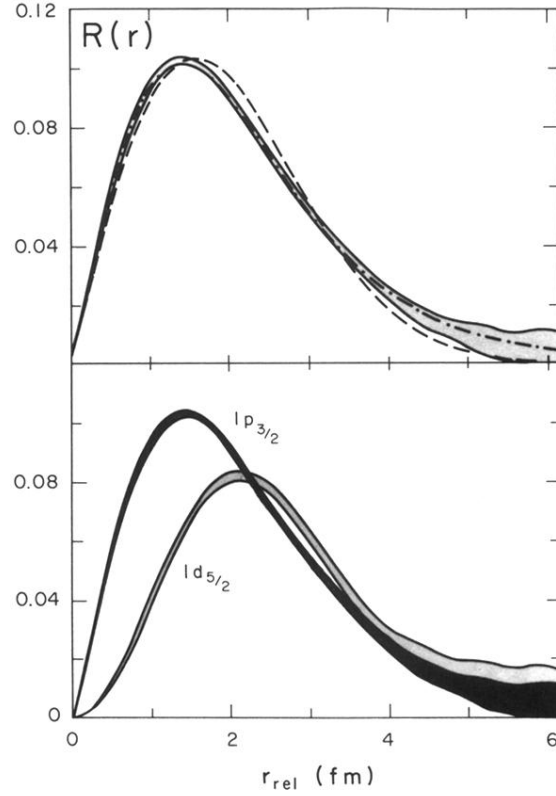


FIG. 2. Top: The shaded band represents the $1p_{3/2}$ single-particle wave function extracted from the measured 1.74-MeV $M3$ form factor in ^{10}B . The width of the band indicates the error due to the statistical uncertainties and incompleteness of the measured data (Ref. 16). The dashed curve shows the harmonic-oscillator shape ($b_{rel} = 1.60$ fm); the dot-dashed curve is obtained from a Woods-Saxon potential well ($r_{WS} = 1.59$ fm, $a = 0.90$ fm, $V_0 = -91$ MeV, and $V_{s.o.} = 0.0$ MeV). Bottom: Comparison of the deduced $1p_{3/2}$ wave function with the wave function determined for the $1d_{5/2}$ neutron orbit in ^{13}C . The abscissa for both graphs is the relative core-particle separation and the normalization of the wave functions is such that $4\pi \int_0^\infty |R(r)|^2 r^2 dr = 1$.